Study of the decay $\overline{B}^0 \to D^{*+}\omega\pi^-$

B. Aubert,[1] R. Barate,[1] M. Bona,[1] D. Boutigny,[1] F. Couderc,[1] Y. Karyotakis,[1] J. P. Lees,[1] V. Poireau,[1]
V. Tisserand,[1] A. Zghiche,[1] E. Grauges,[2] A. Palano,[3] M. Pappagallo,[3] J. C. Chen,[4] N. D. Qi,[4] G. Rong,[4] P. Wang,[4]
Y. S. Zhu,[4] G. Eigen,[5] I. Ofte,[5] B. Stugu,[5] G. S. Abrams,[6] M. Battaglia,[6] D. N. Brown,[6] J. Button-Shafer,[6]
R. N. Cahn,[6] E. Charles,[6] C. T. Day,[6] M. S. Gill,[6] Y. Groysman,[6] R. G. Jacobsen,[6] J. A. Kadyk,[6] L. T. Kerth,[6]
Yu. G. Kolomensky,[6] G. Kukartsev,[6] G. Lynch,[6] L. M. Mir,[6] P. J. Oddone,[6] T. J. Orimoto,[6] M. Pripstein,[6]
N. A. Roe,[6] M. T. Ronan,[6] W. A. Wenzel,[6] M. Barrett,[7] K. E. Ford,[7] T. J. Harrison,[7] A. J. Hart,[7] C. M. Hawkes,[7]
S. E. Morgan,[7] A. T. Watson,[7] K. Goetzen,[8] T. Held,[8] H. Koch,[8] B. Lewandowski,[8] M. Pelizaeus,[8] K. Peters,[8]
T. Schroeder,[8] M. Steinke,[8] J. T. Boyd,[9] J. P. Burke,[9] W. N. Cottingham,[9] D. Walker,[9] T. Cuhadar-Donszelmann,[10]
B. G. Fulsom,[10] C. Hearty,[10] N. S. Knecht,[10] T. S. Mattison,[10] J. A. McKenna,[10] A. Khan,[11] P. Kyberd,[11]
M. Saleem,[11] L. Teodorescu,[11] V. E. Blinov,[12] A. D. Bukin,[12] V. P. Druzhinin,[12] V. B. Golubev,[12] A. P. Onuchin,[12]
S. I. Serednyakov,[12] Yu. I. Skovpen,[12] E. P. Solodov,[12] K. Yu Todyshev,[12] D. S. Best,[13] M. Bondioli,[13]
M. Bruinsma,[13] M. Chao,[13] S. Curry,[13] I. Eschrich,[13] D. Kirkby,[13] A. J. Lankford,[13] P. Lund,[13] M. Mandelkern,[13]
R. K. Mommsen,[13] W. Roethel,[13] D. P. Stoker,[13] S. Abachi,[14] C. Buchanan,[14] S. D. Foulkes,[15] J. W. Gary,[15]
O. Long,[15] B. C. Shen,[15] K. Wang,[15] L. Zhang,[15] H. K. Hadavand,[16] E. J. Hill,[16] H. P. Paar,[16] S. Rahatlou,[16]
V. Sharma,[16] J. W. Berryhill,[17] C. Campagnari,[17] A. Cunha,[17] B. Dahmes,[17] T. M. Hong,[17] D. Kovalskyi,[17]
J. D. Richman,[17] T. W. Beck,[18] A. M. Eisner,[18] C. J. Flacco,[18] C. A. Heusch,[18] J. Kroseberg,[18] W. S. Lockman,[18]
G. Nesom,[18] T. Schalk,[18] B. A. Schumm,[18] A. Seiden,[18] P. Spradlin,[18] D. C. Williams,[18] M. G. Wilson,[18]
J. Albert,[19] E. Chen,[19] A. Dvoretskii,[19] D. G. Hitlin,[19] I. Narsky,[19] T. Piatenko,[19] F. C. Porter,[19] A. Ryd,[19]
A. Samuel,[19] R. Andreassen,[20] G. Mancinelli,[20] B. T. Meadows,[20] M. D. Sokoloff,[20] F. Blanc,[21] P. C. Bloom,[21]
S. Chen,[21] W. T. Ford,[21] J. F. Hirschauer,[21] A. Kreisel,[21] U. Nauenberg,[21] A. Olivas,[21] W. O. Ruddick,[21]
J. G. Smith,[21] K. A. Ulmer,[21] S. R. Wagner,[21] J. Zhang,[21] A. Chen,[22] E. A. Eckhart,[22] A. Soffer,[22] W. H. Toki,[22]
R. J. Wilson,[22] F. Winklmeier,[22] Q. Zeng,[22] D. D. Altenburg,[23] E. Feltresi,[23] A. Hauke,[23] H. Jasper,[23] B. Spaan,[23]
T. Brandt,[24] V. Klose,[24] H. M. Lacker,[24] W. F. Mader,[24] R. Nogowski,[24] A. Petzold,[24] J. Schubert,[24]
K. R. Schubert,[24] R. Schwierz,[24] J. E. Sundermann,[24] A. Volk,[24] D. Bernard,[25] G. R. Bonneaud,[25] P. Grenier,[25, *]
E. Latour,[25] Ch. Thiebaux,[25] M. Verderi,[25] D. J. Bard,[26] P. J. Clark,[26] W. Gradl,[26] F. Muheim,[26] S. Playfer,[26]
A. I. Robertson,[26] Y. Xie,[26] M. Andreotti,[27] D. Bettoni,[27] C. Bozzi,[27] R. Calabrese,[27] G. Cibinetto,[27] E. Luppi,[27]
M. Negrini,[27] A. Petrella,[27] L. Piemontese,[27] E. Prencipe,[27] F. Anulli,[28] R. Baldini-Ferroli,[28] A. Calcaterra,[28]
R. de Sangro,[28] G. Finocchiaro,[28] S. Pacetti,[28] P. Patteri,[28] I. M. Peruzzi,[28, †] M. Piccolo,[28] M. Rama,[28]
A. Zallo,[28] A. Buzzo,[29] R. Capra,[29] R. Contri,[29] M. Lo Vetere,[29] M. M. Macri,[29] M. R. Monge,[29] S. Passaggio,[29]
C. Patrignani,[29] E. Robutti,[29] A. Santroni,[29] S. Tosi,[29] G. Brandenburg,[30] K. S. Chaisanguanthum,[30] M. Morii,[30]
J. Wu,[30] R. S. Dubitzky,[31] J. Marks,[31] S. Schenk,[31] U. Uwer,[31] W. Bhimji,[32] D. A. Bowerman,[32] P. D. Dauncey,[32]
U. Egede,[32] R. L. Flack,[32] J. R. Gaillard,[32] J .A. Nash,[32] M. B. Nikolich,[32] W. Panduro Vazquez,[32] X. Chai,[33]
M. J. Charles,[33] U. Mallik,[33] N. T. Meyer,[33] V. Ziegler,[33] J. Cochran,[34] H. B. Crawley,[34] L. Dong,[34] V. Eyges,[34]
W. T. Meyer,[34] S. Prell,[34] E. I. Rosenberg,[34] A. E. Rubin,[34] A. V. Gritsan,[35] M. Fritsch,[36] G. Schott,[36]
N. Arnaud,[37] M. Davier,[37] G. Grosdidier,[37] A. Höcker,[37] F. Le Diberder,[37] V. Lepeltier,[37] A. M. Lutz,[37]
A. Oyanguren,[37] S. Pruvot,[37] S. Rodier,[37] P. Roudeau,[37] M. H. Schune,[37] A. Stocchi,[37] W. F. Wang,[37]
G. Wormser,[37] C. H. Cheng,[38] D. J. Lange,[38] D. M. Wright,[38] C. A. Chavez,[39] I. J. Forster,[39] J. R. Fry,[39]
E. Gabathuler,[39] R. Gamet,[39] K. A. George,[39] D. E. Hutchcroft,[39] D. J. Payne,[39] K. C. Schofield,[39]
C. Touramanis,[39] A. J. Bevan,[40] F. Di Lodovico,[40] W. Menges,[40] R. Sacco,[40] C. L. Brown,[41] G. Cowan,[41]
H. U. Flaecher,[41] D. A. Hopkins,[41] P. S. Jackson,[41] T. R. McMahon,[41] S. Ricciardi,[41] F. Salvatore,[41] D. N. Brown,[42]
C. L. Davis,[42] J. Allison,[43] N. R. Barlow,[43] R. J. Barlow,[43] Y. M. Chia,[43] C. L. Edgar,[43] M. P. Kelly,[43]
G. D. Lafferty,[43] M. T. Naisbit,[43] J. C. Williams,[43] J. I. Yi,[43] C. Chen,[44] W. D. Hulsbergen,[44] A. Jawahery,[44]
C. K. Lae,[44] D. A. Roberts,[44] G. Simi,[44] G. Blaylock,[45] C. Dallapiccola,[45] S. S. Hertzbach,[45] X. Li,[45] T. B. Moore,[45]
S. Saremi,[45] H. Staengle,[45] S. Y. Willocq,[45] R. Cowan,[46] K. Koeneke,[46] G. Sciolla,[46] S. J. Sekula,[46] M. Spitznagel,[46]
F. Taylor,[46] R. K. Yamamoto,[46] H. Kim,[47] P. M. Patel,[47] C. T. Potter,[47] S. H. Robertson,[47] A. Lazzaro,[48]
V. Lombardo,[48] F. Palombo,[48] J. M. Bauer,[49] L. Cremaldi,[49] V. Eschenburg,[49] R. Godang,[49] R. Kroeger,[49]

J. Reidy,[49] D. A. Sanders,[49] D. J. Summers,[49] H. W. Zhao,[49] S. Brunet,[50] D. Côté,[50] M. Simard,[50] P. Taras,[50]
F. B. Viaud,[50] H. Nicholson,[51] N. Cavallo,[52, ‡] G. De Nardo,[52] D. del Re,[52] F. Fabozzi,[52, ‡] C. Gatto,[52] L. Lista,[52]
D. Monorchio,[52] P. Paolucci,[52] D. Piccolo,[52] C. Sciacca,[52] M. Baak,[53] H. Bulten,[53] G. Raven,[53] H. L. Snoek,[53]
C. P. Jessop,[54] J. M. LoSecco,[54] T. Allmendinger,[55] G. Benelli,[55] K. K. Gan,[55] K. Honscheid,[55] D. Hufnagel,[55]
P. D. Jackson,[55] H. Kagan,[55] R. Kass,[55] T. Pulliam,[55] A. M. Rahimi,[55] R. Ter-Antonyan,[55] Q. K. Wong,[55]
N. L. Blount,[56] J. Brau,[56] R. Frey,[56] O. Igonkina,[56] M. Lu,[56] R. Rahmat,[56] N. B. Sinev,[56] D. Strom,[56]
J. Strube,[56] E. Torrence,[56] F. Galeazzi,[57] A. Gaz,[57] M. Margoni,[57] M. Morandin,[57] A. Pompili,[57] M. Posocco,[57]
M. Rotondo,[57] F. Simonetto,[57] R. Stroili,[57] C. Voci,[57] M. Benayoun,[58] J. Chauveau,[58] P. David,[58] L. Del Buono,[58]
Ch. de la Vaissière,[58] O. Hamon,[58] B. L. Hartfiel,[58] M. J. J. John,[58] Ph. Leruste,[58] J. Malclès,[58] J. Ocariz,[58]
L. Roos,[58] G. Therin,[58] P. K. Behera,[59] L. Gladney,[59] J. Panetta,[59] M. Biasini,[60] R. Covarelli,[60] M. Pioppi,[60]
C. Angelini,[61] G. Batignani,[61] S. Bettarini,[61] F. Bucci,[61] G. Calderini,[61] M. Carpinelli,[61] R. Cenci,[61] F. Forti,[61]
M. A. Giorgi,[61] A. Lusiani,[61] G. Marchiori,[61] M. A. Mazur,[61] M. Morganti,[61] N. Neri,[61] E. Paoloni,[61] G. Rizzo,[61]
J. Walsh,[61] M. Haire,[62] D. Judd,[62] D. E. Wagoner,[62] J. Biesiada,[63] N. Danielson,[63] P. Elmer,[63] Y. P. Lau,[63] C. Lu,[63]
J. Olsen,[63] A. J. S. Smith,[63] A. V. Telnov,[63] F. Bellini,[64] G. Cavoto,[64] A. D'Orazio,[64] E. Di Marco,[64] R. Faccini,[64]
F. Ferrarotto,[64] F. Ferroni,[64] M. Gaspero,[64] L. Li Gioi,[64] M. A. Mazzoni,[64] S. Morganti,[64] G. Piredda,[64] F. Polci,[64]
F. Safai Tehrani,[64] C. Voena,[64] M. Ebert,[65] H. Schröder,[65] R. Waldi,[65] T. Adye,[66] N. De Groot,[66] B. Franek,[66]
E. O. Olaiya,[66] F. F. Wilson,[66] S. Emery,[67] A. Gaidot,[67] S. F. Ganzhur,[67] G. Hamel de Monchenault,[67]
W. Kozanecki,[67] M. Legendre,[67] B. Mayer,[67] G. Vasseur,[67] Ch. Yèche,[67] M. Zito,[67] W. Park,[68] M. V. Purohit,[68]
A. W. Weidemann,[68] J. R. Wilson,[68] M. T. Allen,[69] D. Aston,[69] R. Bartoldus,[69] P. Bechtle,[69] N. Berger,[69]
A. M. Boyarski,[69] R. Claus,[69] J. P. Coleman,[69] M. R. Convery,[69] M. Cristinziani,[69] J. C. Dingfelder,[69] D. Dong,[69]
J. Dorfan,[69] G. P. Dubois-Felsmann,[69] D. Dujmic,[69] W. Dunwoodie,[69] R. C. Field,[69] T. Glanzman,[69] S. J. Gowdy,[69]
M. T. Graham,[69] V. Halyo,[69] C. Hast,[69] T. Hryn'ova,[69] W. R. Innes,[69] M. H. Kelsey,[69] P. Kim,[69] M. L. Kocian,[69]
D. W. G. S. Leith,[69] S. Li,[69] J. Libby,[69] S. Luitz,[69] V. Luth,[69] H. L. Lynch,[69] D. B. MacFarlane,[69] H. Marsiske,[69]
R. Messner,[69] D. R. Muller,[69] C. P. O'Grady,[69] V. E. Ozcan,[69] A. Perazzo,[69] M. Perl,[69] B. N. Ratcliff,[69]
A. Roodman,[69] A. A. Salnikov,[69] R. H. Schindler,[69] J. Schwiening,[69] A. Snyder,[69] J. Stelzer,[69] D. Su,[69]
M. K. Sullivan,[69] K. Suzuki,[69] S. K. Swain,[69] J. M. Thompson,[69] J. Va'vra,[69] N. van Bakel,[69] M. Weaver,[69]
A. J. R. Weinstein,[69] W. J. Wisniewski,[69] M. Wittgen,[69] D. H. Wright,[69] A. K. Yarritu,[69] K. Yi,[69] C. C. Young,[69]
P. R. Burchat,[70] A. J. Edwards,[70] S. A. Majewski,[70] B. A. Petersen,[70] C. Roat,[70] L. Wilden,[70] S. Ahmed,[71]
M. S. Alam,[71] R. Bula,[71] J. A. Ernst,[71] V. Jain,[71] B. Pan,[71] M. A. Saeed,[71] F. R. Wappler,[71] S. B. Zain,[71]
W. Bugg,[72] M. Krishnamurthy,[72] S. M. Spanier,[72] R. Eckmann,[73] J. L. Ritchie,[73] A. Satpathy,[73] C. J. Schilling,[73]
R. F. Schwitters,[73] J. M. Izen,[74] I. Kitayama,[74] X. C. Lou,[74] S. Ye,[74] F. Bianchi,[75] F. Gallo,[75] D. Gamba,[75]
M. Bomben,[76] L. Bosisio,[76] C. Cartaro,[76] F. Cossutti,[76] G. Della Ricca,[76] S. Dittongo,[76] S. Grancagnolo,[76]
L. Lanceri,[76] L. Vitale,[76] V. Azzolini,[77] F. Martinez-Vidal,[77] Sw. Banerjee,[78] B. Bhuyan,[78] C. M. Brown,[78]
D. Fortin,[78] K. Hamano,[78] R. Kowalewski,[78] I. M. Nugent,[78] J. M. Roney,[78] R. J. Sobie,[78] J. J. Back,[79]
P. F. Harrison,[79] T. E. Latham,[79] G. B. Mohanty,[79] H. R. Band,[80] X. Chen,[80] B. Cheng,[80] S. Dasu,[80] M. Datta,[80]
A. M. Eichenbaum,[80] K. T. Flood,[80] J. J. Hollar,[80] J. R. Johnson,[80] P. E. Kutter,[80] H. Li,[80] R. Liu,[80] B. Mellado,[80]
A. Mihalyi,[80] A. K. Mohapatra,[80] Y. Pan,[80] M. Pierini,[80] R. Prepost,[80] P. Tan,[80] S. L. Wu,[80] Z. Yu,[80] and H. Neal[81]

(The *BABAR* Collaboration)

[1]*Laboratoire de Physique des Particules, F-74941 Annecy-le-Vieux, France*
[2]*Universitat de Barcelona, Facultat de Fisica Dept. ECM, E-08028 Barcelona, Spain*
[3]*Università di Bari, Dipartimento di Fisica and INFN, I-70126 Bari, Italy*
[4]*Institute of High Energy Physics, Beijing 100039, China*
[5]*University of Bergen, Institute of Physics, N-5007 Bergen, Norway*
[6]*Lawrence Berkeley National Laboratory and University of California, Berkeley, California 94720, USA*
[7]*University of Birmingham, Birmingham, B15 2TT, United Kingdom*
[8]*Ruhr Universität Bochum, Institut für Experimentalphysik 1, D-44780 Bochum, Germany*
[9]*University of Bristol, Bristol BS8 1TL, United Kingdom*
[10]*University of British Columbia, Vancouver, British Columbia, Canada V6T 1Z1*
[11]*Brunel University, Uxbridge, Middlesex UB8 3PH, United Kingdom*
[12]*Budker Institute of Nuclear Physics, Novosibirsk 630090, Russia*
[13]*University of California at Irvine, Irvine, California 92697, USA*
[14]*University of California at Los Angeles, Los Angeles, California 90024, USA*
[15]*University of California at Riverside, Riverside, California 92521, USA*
[16]*University of California at San Diego, La Jolla, California 92093, USA*
[17]*University of California at Santa Barbara, Santa Barbara, California 93106, USA*
[18]*University of California at Santa Cruz, Institute for Particle Physics, Santa Cruz, California 95064, USA*

[19] *California Institute of Technology, Pasadena, California 91125, USA*
[20] *University of Cincinnati, Cincinnati, Ohio 45221, USA*
[21] *University of Colorado, Boulder, Colorado 80309, USA*
[22] *Colorado State University, Fort Collins, Colorado 80523, USA*
[23] *Universität Dortmund, Institut für Physik, D-44221 Dortmund, Germany*
[24] *Technische Universität Dresden, Institut für Kern- und Teilchenphysik, D-01062 Dresden, Germany*
[25] *Ecole Polytechnique, LLR, F-91128 Palaiseau, France*
[26] *University of Edinburgh, Edinburgh EH9 3JZ, United Kingdom*
[27] *Università di Ferrara, Dipartimento di Fisica and INFN, I-44100 Ferrara, Italy*
[28] *Laboratori Nazionali di Frascati dell'INFN, I-00044 Frascati, Italy*
[29] *Università di Genova, Dipartimento di Fisica and INFN, I-16146 Genova, Italy*
[30] *Harvard University, Cambridge, Massachusetts 02138, USA*
[31] *Universität Heidelberg, Physikalisches Institut, Philosophenweg 12, D-69120 Heidelberg, Germany*
[32] *Imperial College London, London, SW7 2AZ, United Kingdom*
[33] *University of Iowa, Iowa City, Iowa 52242, USA*
[34] *Iowa State University, Ames, Iowa 50011-3160, USA*
[35] *Johns Hopkins University, Baltimore, Maryland 21218, USA*
[36] *Universität Karlsruhe, Institut für Experimentelle Kernphysik, D-76021 Karlsruhe, Germany*
[37] *Laboratoire de l'Accélérateur Linéaire, IN2P3-CNRS et Université Paris-Sud 11, Centre Scientifique d'Orsay, B.P. 34, F-91898 ORSAY Cedex, France*
[38] *Lawrence Livermore National Laboratory, Livermore, California 94550, USA*
[39] *University of Liverpool, Liverpool L69 7ZE, United Kingdom*
[40] *Queen Mary, University of London, E1 4NS, United Kingdom*
[41] *University of London, Royal Holloway and Bedford New College, Egham, Surrey TW20 0EX, United Kingdom*
[42] *University of Louisville, Louisville, Kentucky 40292, USA*
[43] *University of Manchester, Manchester M13 9PL, United Kingdom*
[44] *University of Maryland, College Park, Maryland 20742, USA*
[45] *University of Massachusetts, Amherst, Massachusetts 01003, USA*
[46] *Massachusetts Institute of Technology, Laboratory for Nuclear Science, Cambridge, Massachusetts 02139, USA*
[47] *McGill University, Montréal, Québec, Canada H3A 2T8*
[48] *Università di Milano, Dipartimento di Fisica and INFN, I-20133 Milano, Italy*
[49] *University of Mississippi, University, Mississippi 38677, USA*
[50] *Université de Montréal, Physique des Particules, Montréal, Québec, Canada H3C 3J7*
[51] *Mount Holyoke College, South Hadley, Massachusetts 01075, USA*
[52] *Università di Napoli Federico II, Dipartimento di Scienze Fisiche and INFN, I-80126, Napoli, Italy*
[53] *NIKHEF, National Institute for Nuclear Physics and High Energy Physics, NL-1009 DB Amsterdam, The Netherlands*
[54] *University of Notre Dame, Notre Dame, Indiana 46556, USA*
[55] *Ohio State University, Columbus, Ohio 43210, USA*
[56] *University of Oregon, Eugene, Oregon 97403, USA*
[57] *Università di Padova, Dipartimento di Fisica and INFN, I-35131 Padova, Italy*
[58] *Universités Paris VI et VII, Laboratoire de Physique Nucléaire et de Hautes Energies, F-75252 Paris, France*
[59] *University of Pennsylvania, Philadelphia, Pennsylvania 19104, USA*
[60] *Università di Perugia, Dipartimento di Fisica and INFN, I-06100 Perugia, Italy*
[61] *Università di Pisa, Dipartimento di Fisica, Scuola Normale Superiore and INFN, I-56127 Pisa, Italy*
[62] *Prairie View A&M University, Prairie View, Texas 77446, USA*
[63] *Princeton University, Princeton, New Jersey 08544, USA*
[64] *Università di Roma La Sapienza, Dipartimento di Fisica and INFN, I-00185 Roma, Italy*
[65] *Universität Rostock, D-18051 Rostock, Germany*
[66] *Rutherford Appleton Laboratory, Chilton, Didcot, Oxon, OX11 0QX, United Kingdom*
[67] *DSM/Dapnia, CEA/Saclay, F-91191 Gif-sur-Yvette, France*
[68] *University of South Carolina, Columbia, South Carolina 29208, USA*
[69] *Stanford Linear Accelerator Center, Stanford, California 94309, USA*
[70] *Stanford University, Stanford, California 94305-4060, USA*
[71] *State University of New York, Albany, New York 12222, USA*
[72] *University of Tennessee, Knoxville, Tennessee 37996, USA*
[73] *University of Texas at Austin, Austin, Texas 78712, USA*
[74] *University of Texas at Dallas, Richardson, Texas 75083, USA*
[75] *Università di Torino, Dipartimento di Fisica Sperimentale and INFN, I-10125 Torino, Italy*
[76] *Università di Trieste, Dipartimento di Fisica and INFN, I-34127 Trieste, Italy*
[77] *IFIC, Universitat de Valencia-CSIC, E-46071 Valencia, Spain*
[78] *University of Victoria, Victoria, British Columbia, Canada V8W 3P6*
[79] *Department of Physics, University of Warwick, Coventry CV4 7AL, United Kingdom*
[80] *University of Wisconsin, Madison, Wisconsin 53706, USA*
[81] *Yale University, New Haven, Connecticut 06511, USA*

We report on a study of the decay $\overline{B}^0 \to D^{*+}\omega\pi^-$ with the BABAR detector at the PEP-II B-factory at the Stanford Linear Accelerator Center. Based on a sample of 232 million $B\overline{B}$ decays, we measure the branching fraction $\mathcal{B}(\overline{B}^0 \to D^{*+}\omega\pi^-) = (2.88 \pm 0.21(\text{stat.}) \pm 0.31(\text{syst.})) \times 10^{-3}$. We study the invariant mass spectrum of the $\omega\pi^-$ system in this decay. This spectrum is in good agreement with expectations based on factorization and the measured spectrum in $\tau^- \to \omega\pi^-\nu_\tau$. We also measure the polarization of the D^{*+} as a function of the $\omega\pi^-$ mass. In the mass region 1.1 to 1.9 GeV we measure the fraction of longitudinal polarization of the D^{*+} to be $\Gamma_L/\Gamma = 0.654 \pm 0.042(\text{stat.}) \pm 0.016(\text{syst.})$. This is in agreement with the expectations from heavy-quark effective theory and factorization assuming that the decay proceeds as $\overline{B}^0 \to D^{*+}\rho(1450)$, $\rho(1450) \to \omega\pi^-$.

I. INTRODUCTION

Factorization is a powerful tool to describe hadronic decays of the B-meson. According to factorization, the matrix element of four-quark operators can be written as the product of matrix elements of two two-quark operators [1]. Thus, the process $b \to cW^*$, $W^* \to q\bar{q}'$ (where $q = d$ or s, $q' = u$ or c) can be "broken up" into two pieces, the $b \to c$ transition and the hadronization from $W^* \to q\bar{q}'$ decay.

Ligeti, Luke, and Wise have proposed an elegant test of factorization [2]. In this test, data from $\tau \to X\nu$, where X is a hadronic system, is used to predict the properties of $B \to D^*X$ (see Fig. 1). If X is composed of two or more particles not dominated by a single narrow resonance, factorization can be tested in different kinematic regions.
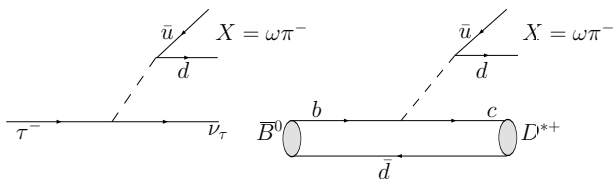

FIG. 1: Feynman diagrams for $\tau \to \omega\pi\nu$ and $\overline{B}^0 \to D^{*+}\omega\pi^-$.

In the event that X is a multi-body system, it is possible that some fraction of the hadronic system could be emitted in association with the $B \to D^{(*)}$ transition instead of the hadronization from $W^* \to q\bar{q}'$ decay. In the case of $X \equiv \omega\pi^-$, the pion must come from the W^* to conserve charge. It is unlikely that the ω could be produced from the lower vertex in Fig. 1 [2, 3]. Furthermore the $\omega\pi^-$ state is not associated with any narrow resonance, so that a wide range in $\omega\pi^-$ invariant mass can be studied. As the branching fraction for $\overline{B}^0 \to D^{*+}\omega\pi^-$

is large ($\approx 0.3\%$), this decay provides a good laboratory for the study of factorization.

The branching fraction for $\overline{B}^0 \to D^{*+}\omega\pi^-$ has been measured by the CLEO collaboration, using a sample of 9.7 million $B\bar{B}$ pairs collected at the $\Upsilon(4S)$ resonance, to be $(2.9 \pm 0.3(\text{stat.}) \pm 0.4(\text{syst.})) \times 10^{-3}$ [4]. They also extracted the spectrum of m_X^2, the square of the invariant mass of the $\omega\pi$ system. This spectrum is found to be in agreement with theoretical expectations [2]. In addition, the CLEO collaboration studied the related decay $B \to D\omega\pi$ and concluded that this decay is dominated by the broad $\rho(1450)$ intermediate resonance; i.e., $B \to D\rho(1450)$, $\rho(1450) \to \omega\pi$. Assuming that this intermediate state also dominates in $\overline{B}^0 \to D^{*+}\omega\pi^-$, factorization can be used to predict the polarization of the D^* with the aid of heavy-quark effective theory (HQET) and data from semileptonic B-decays [5]. These predictions are in agreement with the CLEO result for the longitudinal polarization fraction, $\Gamma_L/\Gamma = (63 \pm 9)\%$ [4].

In this paper we study the decay $\overline{B}^0 \to D^{*+}\omega\pi^-$ with a larger sample of B decays than available in the original CLEO study. We present measurements of the branching fraction, the Dalitz plot distribution, the m_X^2 spectrum, the $m_{D^*\pi}$ distribution, and the D^* polarization as a function of m_X.

II. THE BABAR DATASET AND DETECTOR

The results presented in this paper are based on 232×10^6 $\Upsilon(4S) \to B\overline{B}$ decays, corresponding to an integrated luminosity of 211 fb^{-1}. The data were collected between 1999 and 2004 with the BABAR detector [6] at the PEP-II B Factory at SLAC. In addition a 22 fb^{-1} off-resonance data sample, with center-of-mass energy 40 MeV below the $\Upsilon(4S)$ resonance, is used to study backgrounds from continuum events, $e^+e^- \to q\bar{q}$ ($q = u, d, s$, or c).

Charged-particle tracking is provided by a five-layer double-sided silicon vertex tracker (SVT) and a 40-layer drift chamber (DCH), operating within a 1.5-T magnetic field. Energy depositions are measured with a CsI(Tl) electromagnetic calorimeter (EMC). Charged particles are identified from ionization energy loss ($\mathrm{d}E/\mathrm{d}x$) measurements in the SVT and DCH, and from the observed pattern of Cherenkov light in an internally reflecting ring

*Also at Laboratoire de Physique Corpusculaire, Clermont-Ferrand, France
†Also with Università di Perugia, Dipartimento di Fisica, Perugia, Italy
‡Also with Università della Basilicata, Potenza, Italy

imaging detector.

III. ANALYSIS STRATEGY

Starting from the set of reconstructed charged tracks and energy deposits within the EMC, we select events that are kinematically consistent with $\overline{B}^0 \to D^{*+}\omega\pi^-$ in the following decay modes: $D^{*+} \to D^0\pi^+$, with $D^0 \to K^-\pi^+$, $K^-\pi^+\pi^+\pi^-$, or $K^-\pi^+\pi^0$, and $\omega \to \pi^+\pi^-\pi^0$. Charge-conjugate modes are implied throughout this paper.

In the reconstruction chain, the invariant mass requirement on the $\pi^+\pi^-\pi^0$ system that forms the ω candidate is kept loose. We then select "signal" or "sideband" candidates depending on whether the reconstructed $\pi^+\pi^-\pi^0$ mass is consistent with the ω hypothesis. Kinematic distributions of interest, such as the m_X^2 spectrum, are obtained by subtracting, with appropriate weights, the distributions for signal and sideband events. This subtraction accounts for all sources of backgrounds, including backgrounds from $\overline{B}^0 \to D^{*+}\pi^-\pi^+\pi^-\pi^0$, on a statistical basis. This is because, as we will demonstrate in Section VI, background sources with real ω decays are negligible.

The event reconstruction efficiency is determined from simulated Monte Carlo events, where the response of the *BABAR* detector is modeled using the GEANT4 [7] program. Efficiency-corrected kinematic distributions are obtained by assigning a weight to each event. This weight is equal to the inverse of the efficiency to reconstruct that particular event given its kinematic properties. This procedure, which is independent of assumptions on the dynamics of the $\overline{B}^0 \to D^{*+}\omega\pi^-$ decay, is discussed in Section VII.

IV. EVENT SELECTION CRITERIA

The event selection criteria are optimized based on studies of off-resonance data, and simulated $B\bar{B}$ and continuum events.

Photon candidates are constructed from calorimeter clusters with lateral profiles consistent with photon showers and with energies above 30 MeV. Neutral pion candidates are formed from pairs of photon candidates with invariant mass between 115 and 150 MeV and energy above 200 MeV, where the π^0 mass resolution is 6.5 MeV. In order to improve resolution, $\pi^0 \to \gamma\gamma$ candidates are constrained to the world average π^0 mass [8].

The kaon-candidate track used to reconstruct the D^0 meson must satisfy a set of kaon identification criteria. The kaon identification efficiency depends on momentum and polar angle, and is typically about 93%. These requirements provide a rejection factor of order 10 against pions. For each $D^0 \to K^-\pi^+\pi^0$ candidate, we calculate the square of the decay amplitude ($|A|^2$) based on the

kinematics of the decay products and the known properties of the Dalitz plot for this decay [9]. We retain candidates if $|A|^2$ is greater than 2% of its maximum possible value. The efficiency of this requirement is 91%. Finally, the measured invariant mass of D^0 candidates must be within 15 MeV of the world average D^0 mass [8] for $D^0 \to K^-\pi^+$ and $D^0 \to K^-\pi^+\pi^-\pi^-$, and 25 MeV for $D^0 \to K^-\pi^+\pi^0$. The experimental resolution is about 6 MeV for $D^0 \to K^-\pi^+$, $K^-\pi^+\pi^-\pi^-$, and 10 MeV for $D^0 \to K^-\pi^+\pi^0$.

We select D^{*+} candidates by combining D^0 candidates with an additional track, assumed to correspond to a pion. We require the measured mass difference $\Delta m \equiv m(D^{*+}) - m(D^0)$ to be between 143.4 and 147.4 MeV. The resolution on this quantity is 0.3 MeV with non-Gaussian behavior due to the reconstruction of the low momentum pion from D^* decay.

In the rest frame of the $\overline{B}^0$, as m_X^2 increases the D^{*+} is produced with decreasing energy. At high m_X^2, or equivalently low D^{*+} energy, the reconstruction efficiency drops as $\cos\theta_D \to 1$, where θ_D is the angle between the daughter D^0 and the direction opposite the flight of the $\overline{B}^0$ in the D^{*+} rest frame. We exclude the region of low acceptance ($\cos\theta_D > 0.8$ for $8 \le m_X^2 < 9$ GeV^2, $\cos\theta_D > 0.6$ for $9 \le m_X^2 < 10$ GeV^2, and $\cos\theta_D > 0.4$ for $m_X^2 \ge 10$ GeV^2) from our event selection. The effect on the final results is very small, as will be discussed in Section VIII.

We form ω candidates from a pair of oppositely-charged tracks, assumed to be a $\pi^+\pi^-$ pair, and a π^0 candidate. In order to keep signal and sideband candidates (see Section III) we impose only the very loose requirement that the invariant mass of the ω candidate be within 70 MeV of the world average ω mass [8]. (The natural width of the ω resonance is 8.5 MeV and the experimental resolution is 5.6 MeV.)

In order to reduce combinatoric backgrounds, we impose a requirement on the kinematics of the ω decay [10]. This is done by first defining two Dalitz plot coordinates: $X \equiv 3T_0/Q - 1$ and $Y \equiv \sqrt{3}(T_+ - T_-)/Q$, where $T_{\pm,0}$ are the kinetic energies of the pions in the ω rest frame and $Q \equiv T_+ + T_- + T_0$. Next, we define the normalized square of the distance from the center of the Dalitz plot, $R^2 \equiv (X^2 + Y^2)/(X_b^2 + Y_b^2)$, where X_b and Y_b are the coordinates of the intersection between the kinematic boundary of the Dalitz plot and a line passing through $(0,0)$ and (X,Y). Since the Dalitz plot density for real ω decays peaks at $R = 0$, we impose the requirement $R < 0.85$. This requirement is 93% efficient for signal and rejects 25% of the combinatorial background.

We reconstruct a B-meson candidate by combining a D^{*+} candidate, an ω candidate, and an additional negatively charged track. A B-candidate is characterized kinematically by the energy-substituted mass $m_{\mathrm{ES}} \equiv \sqrt{(\frac{1}{2}s + \vec{p}_0 \cdot \vec{p}_B)^2/E_0^2 - p_B^2}$, where E and p denote energy and momentum measured in the lab frame, the subscripts 0 and B refer to the initial $\Upsilon(4S)$ and B candidate, respectively, and s represents the square of the energy of the e^+e^- center of mass (CM) system. For signal events

we expect $m_{\mathrm{ES}} \approx M_B$ within the experimental resolution of about 3 MeV, where M_B is the world average B mass [8]. In the same fashion, the energy difference $\Delta E \equiv E_B^* - \frac{1}{2}\sqrt{s}$, where the asterisk denotes the CM frame, is expected to be nearly zero for signal B decays.

The ΔE resolution is approximately 25 MeV in the $K^-\pi^+\pi^0$ mode and 20 MeV in the other modes, with non-Gaussian tails towards negative values due to energy leakage in the EMC. We select B candidates with a $D^0 \to K^-\pi^+\pi^0$ as long as $-70 \le \Delta E \le 40$ MeV, and we require $-50 \le \Delta E \le 35$ MeV for the other modes.

In order to further reduce the number of events from continuum backgrounds we make two additional requirements. First, we require $|\cos\theta_B| < 0.9$, where θ_B is the decay angle of the B candidate with respect to the e^- beam direction in the CM frame. For real B candidates, $\cos\theta_B$ follows a $1-x^2$ distribution, while the distribution is essentially flat for B candidates formed from random combinations of tracks. Second, we impose a requirement on a Fisher discriminant [11] designed to differentiate between spherical $B\bar{B}$ events and jet-like continuum events. This discriminant is constructed from the quantities $L_0 = \sum_i p_i^*$ and $L_2 = \sum_i p_i^* \cos^2\alpha_i^*$. Here, p_i^* is the magnitude of the momentum and α_i^* is the angle with respect to the thrust axis of the B candidate of tracks and clusters not used to reconstruct the B, all in the CM frame. The requirements on $|\cos\theta_B|$ and the Fisher discriminant are 95% efficient for signal and reject nearly 40% of the continuum background.

The reconstruction of the $\overline{B}^0 \to D^{*+}\omega\pi^-$ decay is improved by refitting the momenta of the decay products of the $\overline{B}^0$, taking into account kinematic and geometric constraints. The kinematic constraints are based on the fact that their decay products must originate from a common point in space. The entire decay chain is fit simultaneously in order to account for any correlations between intermediate particles.

If more than one B candidate is found in a given event with $m_{\mathrm{ES}} > 5.2$ GeV, and passes selection requirements, we retain the best candidate based on a χ^2 algorithm that uses the measured values, world average values, and resolutions of the D^0 mass and the mass difference Δm. We omit the ω candidate mass information from arbitration in order to avoid introducing a bias in the ω mass distribution, since this distribution is used extensively throughout the analysis.

V. EVENT YIELD

In Fig. 2 we show the m_{ES} distribution for candidates with reconstructed $\pi^+\pi^-\pi^0$ mass (m_ω) in the signal and sideband regions, which are defined as $|m_\omega - m_\omega^{PDG}| < 20$ MeV and $35 < |m_\omega - m_\omega^{PDG}| < 70$ MeV, respectively, where m_ω^{PDG} is the world average ω mass [8].

The m_{ES} distribution for the m_ω signal region has been fitted to the sum of a threshold background function [12] and a Gaussian distribution centered at M_B. The dis-
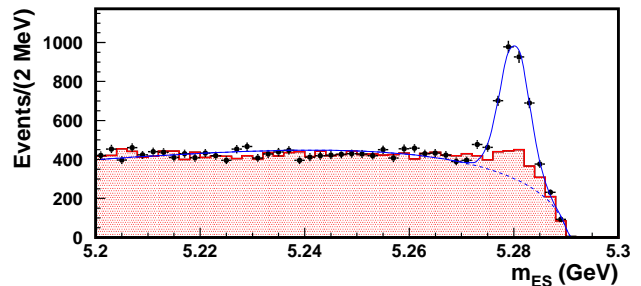

FIG. 2: m_{ES} distributions for candidates with reconstructed ω mass in the signal (points) and sideband (shaded histogram) regions. The distribution for events in the sideband region has been rescaled to match the expected background in the m_ω signal region. The fitted function is described in the text.

tribution for the m_ω sideband region demonstrates the presence of a background component, which peaks in m_{ES} but not in m_ω, that is not well described by the threshold function. Monte Carlo studies indicate that approximately one-third of this component is due to signal events where the ω is mis-reconstructed. These are, for example, events where one of the pion tracks in the ω decay is lost and is replaced by a track from the decay of the other B in the event. The remaining two-thirds of the m_{ES} peaking background component is due to $\overline{B}^0 \to D^{*+}\pi^+\pi^-\pi^0\pi^-$ events.

We extract the event yield from a binned χ^2 fit of the m_ω distribution for events with $m_{\mathrm{ES}} > 5.27$ GeV. The data distribution is modelled as the sum of a Voigtian function and a linear background function. (The Voigtian is the convolution of a Breit-Wigner with a Gaussian resolution function.) The width of the Breit-Wigner is fixed at 8.5 MeV, the world average width of the ω. The mass of the ω, the Gaussian resolution term, and the parameters of the linear function are free in the fit.

The m_ω distribution and the associated fit is shown in Fig. 3. The yield, defined as the number of events in the Voigtian with $|m_\omega - m_\omega^{PDG}| < 20$ MeV, is 1799 ± 87 events. The Gaussian resolution returned by the fit as well as the mean of the Breit-Wigner are consistent with the value we find in Monte Carlo simulations of $\overline{B}^0 \to D^{*+}\omega\pi^-$ events. In Fig. 3 we also include the m_ω distribution for events with $5.20 < m_{\mathrm{ES}} < 5.25$ GeV (the m_{ES} sideband). This background distribution has been scaled to the number of background events expected from a fit to the m_{ES} distribution where we require $|m_\omega - m_\omega^{PDG}| < 70$ MeV. The difference between the number of observed events away from the m_ω peak and the number of background events predicted from the m_{ES} sideband is due to the background component that peaks in m_{ES}.

The validity of the yield extraction relies on the assumption that the background is linear in m_ω, and, most importantly, that there are no sources of combinatoric backgrounds that include real ω decays. The results shown in Fig. 3 imply that there is no significant com-
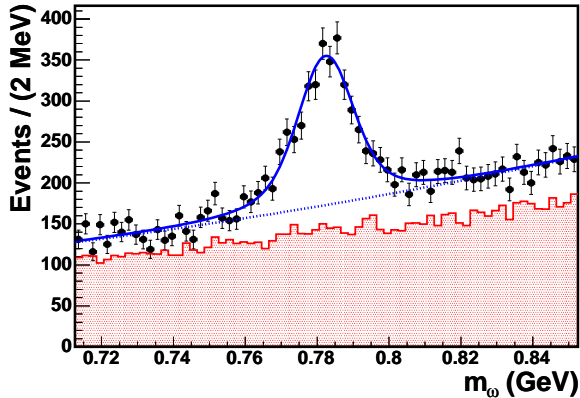
FIG. 3: Distribution of reconstructed m_ω for events with $m_{\rm ES} > 5.27$ GeV (points) and events with $5.20 < m_{\rm ES} < 5.25$ GeV (shaded histogram). The superimposed fit is described in the text. The events from the $m_{\rm ES}$ sideband have been scaled to the expected background from an $m_{\rm ES}$ fit to events with $|m_\omega - m_\omega^{PDG}| < 70$ MeV (*i.e.*, the range shown in this figure).

ponent of real ω decays in the background. To verify this, we have examined and fit the m_ω distribution for data events in the $m_{\rm ES}$ sideband as well as the distribution for Monte Carlo simulations of $B\bar{B}$ events, excluding $\overline{B}^0 \to D^{*+}\omega\pi^-$. We find that the distributions are well modelled by linear functions. There is no evidence of a real ω component in the background. We estimate that this component can affect the yield extraction of Fig. 3 at most at the few percent level.

We also divide our dataset into three independent sub-datasets, according to the three D^0 decay modes that we consider. The fits to these sub-datasets yield consistent results.

VI. BACKGROUND SUBTRACTION

In this work we are interested in studying a number of kinematic distributions for $\overline{B}^0 \to D^{*+}\omega\pi^-$, such as the m_X^2 distribution, where m_X is the invariant mass of the $\omega\pi$ system. The measurements of these distributions need to account for the presence of background in the sample and for the fact that the signal reconstruction efficiency is not constant over the Dalitz plot.

We use distributions for ω sideband events to remove the effects of the background in the ω signal region on a statistical basis, and we use Monte Carlo simulations to correct for efficiency effects. This is accomplished as follows:

1. The simulation of $\overline{B}^0 \to D^{*+}\omega\pi^-$ events is used to calculate the signal reconstruction efficiency $\epsilon(\vec{x})$, where $\vec{x}$ is the set of quantities that specify the

kinematics of a given event. The procedure used to determine $\epsilon(\vec{x})$ is discussed in Section VII.

2. In the absence of background, we would calculate the number of events corrected for efficiency in a given bin of m_X^2 as

$$N(m_X^2) = \sum_{\rm signal} \frac{1}{\epsilon(\vec{x}_i)}, \qquad (1)$$

where the sum is over signal events in a given m_X^2 bin and $\vec{x}_i$ is the set of kinematic quantities for the i-th event in the sum.

3. As mentioned above, the background subtraction is performed using the m_ω sideband. Thus, Eq. 1 is modified to be

$$N(m_X^2) = \sum_{\rm signal} \frac{1}{\epsilon(\vec{x}_i)} \ - \ \frac{4}{7}\beta \sum_{\rm sideband} \frac{1}{\epsilon(\vec{x}_j)} \qquad (2)$$

where the first sum is just as before, while the second sum is over ω-mass sideband events in the given bin of m_X^2 and $\vec{x}_j$ represents the set of kinematic quantities for the j-th event in the sideband event sample. The same efficiency is used for both the signal and sideband event samples. The factor of $\frac{4}{7}$ is needed to adjust for the relative size of the ω signal and sideband regions. The additional factor of β is ideally equal to one, and it is introduced to correct for any possible bias in the background subtraction procedure, as will be discussed below.

The allowed kinematic limits for some variables, such as m_X^2, are not the same for ω signal and sideband events. Therefore, the values of these variables for events in the ω sideband region are linearly rescaled so that their kinematic limits match the kinematic limits for events in the ω signal region. This procedure is necessary to avoid the introduction of artificial structures in background-subtracted distributions for these variables near the kinematic limits.

We test the sideband subtraction algorithm on a number of background samples such as Monte Carlo $B\bar{B}$ events and data events in sidebands of $m_{\rm ES}$ and ΔE. These tests are performed using the efficiency parametrization discussed in Section VII. We find that background-subtracted kinematic distributions in the background samples show no significant structure. One sample distribution is shown in Fig. 4. We find a small bias in the extraction of the background-subtracted yields if the parameter β in Eq. 2 is set to unity. To correct for this bias we set $\beta = 0.975$, with an estimated systematic uncertainty of ± 0.010.

VII. EFFICIENCY PARAMETRIZATION

The process of interest ($\overline{B}^0 \to D^{*+}\omega\pi^-$) is the three-body decay of a pseudoscalar particle into two vector
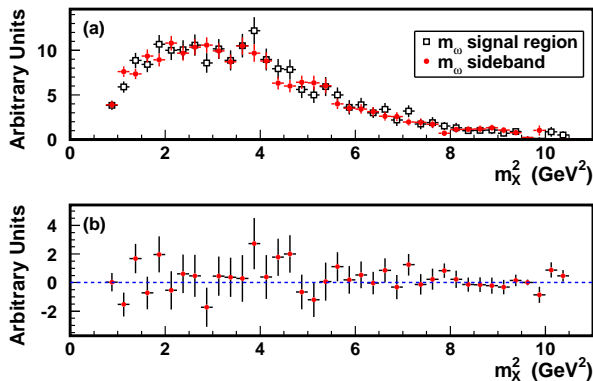
FIG. 4: (a) Efficiency-corrected m_X^2 distributions for events from the m_{ES} sideband with reconstructed m_ω in the signal and sideband regions (arbitrary units). The distribution for events in the sideband region has been scaled by a factor of $\frac{4}{7}$. (b) Background subtracted m_X^2 distribution for events from the m_{ES} sideband (arbitrary units). This distribution has been obtained by subtracting the two distributions in (a).

The functions ϵ', c_1, and c_2 are extracted from Monte Carlo simulations and tabulated as a set of two dimensional histograms. As an example, the ϵ' distribution for events with $D^0 \to K^-\pi^+$ is given in Fig. 5.

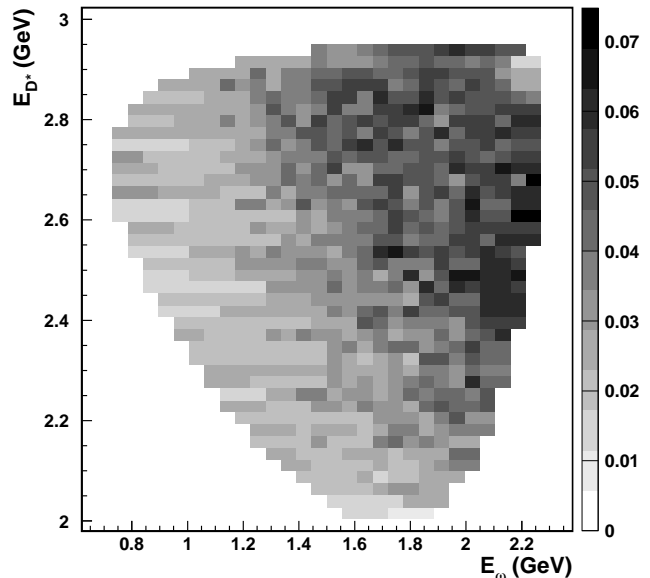FIG. 5: The $\epsilon'(D^0 \to K^-\pi^+, E_\omega, E_{D^*})$ distribution for $\overline{B}^0 \to D^{*+}\omega\pi^-$ Monte Carlo events.

particles and a pseudoscalar particle. We parametrize the reconstruction efficiency as a function of five variables:

1. d, an index that labels the decay mode of the D^0; i.e., $D^0 \to K^-\pi^+$, $K^-\pi^+\pi^+\pi^-$, or $K^-\pi^+\pi^0$;

2. E_ω, the energy of the ω in the $\overline{B}^0$ rest frame;

3. E_{D^*}, the energy of the D^* in the $\overline{B}^0$ rest frame;

4. $\cos\theta_D$, the cosine of the decay angle of the D^*; i.e., the angle between the D^0 and the direction opposite the flight of the $\overline{B}^0$ in the D^{*+} rest frame.

5. $\cos\alpha$, the cosine of the angle between the vector normal to the ω decay plane and the direction opposite the flight of the $\overline{B}^0$, measured in the ω rest frame.

Note that two other variables would be needed to fully describe the kinematics of the decay chain. These are the angles that define, in addition to $\cos\theta_D$ and $\cos\alpha$, the orientation between the decay planes of the D^* and the ω and the decay plane of the $\overline{B}^0$. Monte Carlo studies show that the reconstruction efficiency is independent of these two variables. The E_ω and E_{D^*} variables are the usual Dalitz variables used to describe three-body decays. Because of energy-momentum conservation the E_ω and E_{D^*} variables are equivalent in information content to the squared invariant masses of the $D^*\pi$ ($m_{D^*\pi}^2$) and $\omega\pi$ (m_X^2) systems respectively.

The efficiency is then parametrized as

$$\begin{aligned}\epsilon(\vec{x}_i) &= \epsilon(E_\omega, E_{D^*}, \cos\theta_D, |\cos\alpha|; d) \\ &= \epsilon'(E_\omega, E_{D^*}; d) \cdot c_1(E_\omega, |\cos\alpha|) \cdot c_2(E_{D^*}, \cos\theta_D; d).\end{aligned} \quad (3)$$

The efficiency parametrization is validated using samples of Monte Carlo signal events. These samples are generated with a variety of ad-hoc kinematic properties; e.g., different polarizations for the D^* and the ω, different shapes of the m_X^2 distribution. In all cases we find that the shapes of kinematic distributions are well reproduced after the efficiency correction.

We use the following method to estimate the effect of the finite statistics of the Monte Carlo sample. We generate a set of 400 new ϵ', c_1, and c_2 templates based on the nominal templates obtained from Monte Carlo signal events. If the measured efficiency in a given bin of the nominal template is $\mu \pm \sigma$, the corresponding efficiencies in the new templates are drawn from a Gaussian distribution of mean μ and standard deviation σ. Then, the measurement of any quantity of interest (e.g., m_X^2) is repeated 400 times, according to Eq. 2, using the new templates. The spread in the results obtained from events reconstructed in data is a measure of the systematic uncertainty due to the finite number of available Monte Carlo events. This spread is then added in quadrature to the statistical uncertainty of our results.

We observe a small bias in the total number of reconstructed signal events obtained from the efficiency correction. This is due to the fact that, although the uncertainty on $\epsilon(\vec{x}_i)$ is Gaussian, the factor $1/\epsilon(\vec{x}_i)$ used in the efficiency correction procedure (Eqs. 1, 2) does not

obey Gaussian statistics. As a result, after applying the efficiency correction, the total number of reconstructed events tends to slightly overestimate the true value.

In order to quantify this bias on the nominal result due to the finite number of Monte Carlo signal events, we first determine the mean of the total number of reconstructed signal events in data for the 400 new efficiency templates. This mean differs from the nominal result by a few percent (δ). We then repeat the procedure described above using events reconstructed from signal Monte Carlo. We use the results of these Monte Carlo studies to describe the bias as a function of δ. We find that after applying the efficiency correction and subtracting the m_ω side-band, the total number of events reconstructed using signal Monte Carlo exceeds the true value by $(0.6 \pm 0.4) \cdot \delta$. We correct our final results by this amount.

VIII. RESULTS

We use the procedure outlined above, with one additional correction, to extract the branching fraction, the m_X^2 distribution, the Dalitz plot distribution, the $m_{D^*\pi}$ distribution, and the polarization of the D^* as a function of m_X. The one additional correction accounts for the region of phase space with low acceptance that was excluded from the analysis. This region corresponds to values of $\cos\theta_D$ near 1 for low E_D^*, or equivalently high m_X^2. This correction factor varies between approximately 1.2 at $m_X^2 = 8$ GeV^2 and 1.6 at $m_X^2 = 11$ GeV^2. Since most of the data is at $m_X^2 < 4$ GeV^2, the combined effect of this correction is quite small; it amounts to an increase of less than 1% relative to the measured branching fraction.

For the branching fraction, we find $\mathcal{B}(\overline{B}^0 \rightarrow D^{*+}\omega\pi^-) = (2.88 \pm 0.21(\text{stat.}) \pm 0.31(\text{syst.})) \times 10^{-3}$. The total systematic uncertainty of 10.8% arises from the following sources:

- The uncertainties in the branching fractions of the D^*, D, and ω: 5%.

- The uncertainty in the reconstruction efficiency of neutral pions at *BABAR*, which is estimated to be 3% per π^0. This amounts to a 6% uncertainty for events reconstructed with $D^0 \rightarrow K^-\pi^+\pi^0$, and 3% for the other modes. Combining these modes, the systematic uncertainty from this source is 4.3%.

- The uncertainty in the reconstruction efficiency for charged tracks. From a variety of control samples, this is estimated to be 0.6% (0.8%) for each track of transverse momentum above (below) 200 MeV. Including the uncertainty for the low momentum pion produced in the D^{*+} decay, we obtain a systematic uncertainty of 5.3%.

- The uncertainty in the efficiency of the kaon particle identification requirements: 2%.

- The uncertainty due to the limited Monte Carlo sample size in the efficiency calculation: 3.8%.

- The uncertainty on the quantity β in Eq. 2: 2.6%.

- The uncertainty in the efficiency of the various event selection criteria, estimated to be 4.3%.

- The uncertainty in the number of $B\bar{B}$ events in the *BABAR* event sample: 1.1%.

- The uncertainty in the correction due to the removal of events at high $\cos\theta_D$ and small E_{D^*}: 0.3%.

Some of these systematic uncertainties vary as a function of m_X^2. For example, the uncertainty on the correction due to removing a region of $(E_{D^*}, \cos\theta_D)$ phase space is only relevant to events with m_X^2 above 8 GeV^2. A portion of the systematic uncertainty due to limited Monte Carlo sample size also varies as a function of m_X^2. Therefore, quantities measured as a function of m_X^2 include a common scale uncertainty of 10.5% and a systematic uncertainty that varies with m_X^2 and is typically below a few percent.

The m_X^2 distribution, normalized to the semileptonic width $\Gamma(B \rightarrow D^*\ell\nu)$ [8], is shown in Fig. 6. A scale uncertainty on our result of 11.3% is not shown. This uncertainty combines a 4.2% uncertainty in $\Gamma(B \rightarrow D^*\ell\nu)$ with the 10.5% uncertainty from the sources listed above. The bulk of the data is concentrated in a broad peak around $m_X^2 \approx 2$ GeV^2, in the region of $\rho(1450) \rightarrow \omega\pi$. Our distribution agrees well in both shape and normalization with predictions based on factorization and τ decay data [13] in the region $m_X^2 \leq 2.8$ GeV^2 covered by the tau data.

The background-subtracted and efficiency-corrected Dalitz plot is shown in Fig. 7. One notable feature of the decay distribution is an enhancement for $D^*\pi$ masses near 2.5 GeV ($m_{D^*\pi}^2 \sim 6.3$ GeV^2). The enhancement occurs in the region where one expects to find a broad $J = 1$ D^{**} resonance (D_1') that decays via S-wave to $D^*\pi$. Thus, this enhancement could be due to the color-suppressed decay $\overline{B}^0 \rightarrow D_1'\omega$, followed by $D_1' \rightarrow D^{*+}\pi^-$.

In Fig. 8 we show the background-subtracted and efficiency-corrected $D^*\pi$ mass distribution for events away from the $\rho(1450)$ peak, fitted to the sum of a fourth order polynomial and a relativistic Breit-Wigner. In this figure, in order to remove the contribution from the $\rho(1450)$, we have required $\cos\theta_{D^*} < 0.5$, where θ_{D^*} is the angle between the momentum of the D^* in the $D^*\pi$ rest frame, and the flight direction of $D^*\pi$ system. We use the $\cos\theta_{D^*}$ variable rather than m_X^2 to remove the $\rho(1450)$ contribution because the distribution in $\cos\theta_{D^*}$ is uniform for S-wave $D_1' \rightarrow D^*\pi$ decay. The yield of possible $\overline{B}^0 \rightarrow D_1'\omega$ events in Fig. 8 can then be easily extrapolated to the full kinematic range. Furthermore, by subdividing the dataset in bins of $\cos\theta_{D^*}$ we can test the S-wave decay hypothesis.

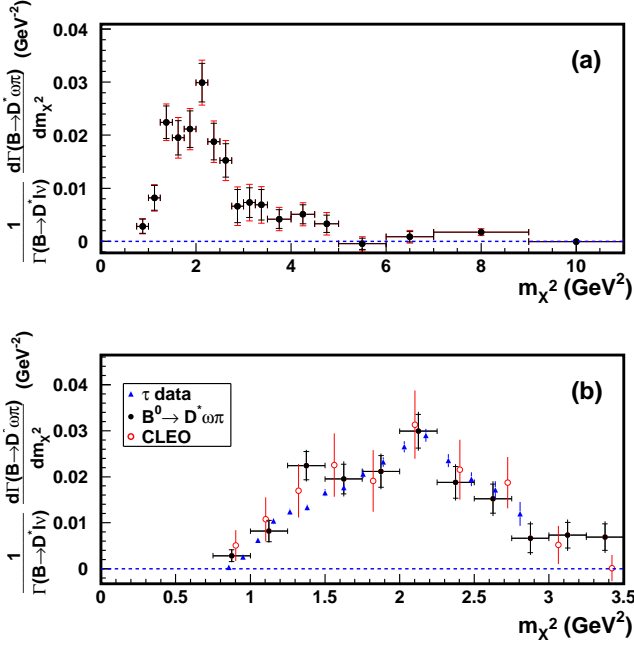The fitted mass and width of the Breit-Wigner in Fig. 8 are 2477 ± 28 MeV and 266 ± 97 MeV, respectively. These

FIG. 6: (a) Data m_X^2 distribution normalized to the semileptonic width $\Gamma(B \to D^*\ell\nu)$. The inner error bars reflect the statistical uncertainties on the data. The total error bars include the m_X^2-dependent systematic uncertainties. A common 11.3% scale systematic uncertainty is not shown. (b) Same as (a) but zoomed-in on the low m_X^2 region, where comparisons based on factorization and τ data can be made. Also shown here are the results from the CLEO analysis [4].

FIG. 7: Background-subtracted and efficiency-corrected Dalitz plot for $B \to D^*\omega\pi$. The relative box sizes indicate the population of the bins. Black boxes indicate positive values, white boxes indicate negative values, which can occur because of statistical fluctuations in the subtraction procedure.

FIG. 8: Background-subtracted and efficiency-corrected $D^*\pi$ mass distribution with $\cos\theta_{D^*} < 0.5$. The superimposed fit is described in the text.

values are consistent with the parameters of the broad $D_1' \to D^*\pi$ resonance observed by the Belle collaboration in $B \to D_1'\pi$ decays, $m = 2427 \pm 36$ MeV and $\Gamma = 384^{+107}_{-75} \pm 74$ MeV [14]. We have also split the data set of Fig. 8 into three equal-sized bins of $\cos\theta_{D^*}$. We find that the fitted amplitude of the Breit-Wigner component is the same, within statistical uncertainties, in the three data sets. This is consistent with expectations for an S-wave $D_1' \to D^*\pi$ decay.

If we assume that the enhancement for $D^*\pi$ masses near 2.5 GeV is actually due to $\overline{B}^0 \to D_1'\omega$, $D_1' \to D^{*+}\pi^-$, we extract the branching fraction

$$\mathcal{B}(\overline{B}^0 \to D_1'\omega) \times \mathcal{B}(D_1' \to D^{*+}\pi^-) =$$
$$(4.1 \pm 1.2 \pm 0.4 \pm 1.0) \times 10^{-4}. \qquad (4)$$

In this measurement, the first uncertainty is statistical, the second uncertainty is from the uncertainties in common with the $\mathcal{B}(\overline{B}^0 \to D^{*+}\omega\pi^-)$ measurement, and the last uncertainty arises from the uncertainties on the choice of the nonresonant shape in Fig. 8 (10%) and the uncertainties in the parameters of the D_1' resonance (22%). This branching fraction has been obtained from fitting the sample of events with $\cos\theta_{D^*} < 0.5$, and scaling up the result by a factor of $\frac{4}{3}$. This procedure neglects
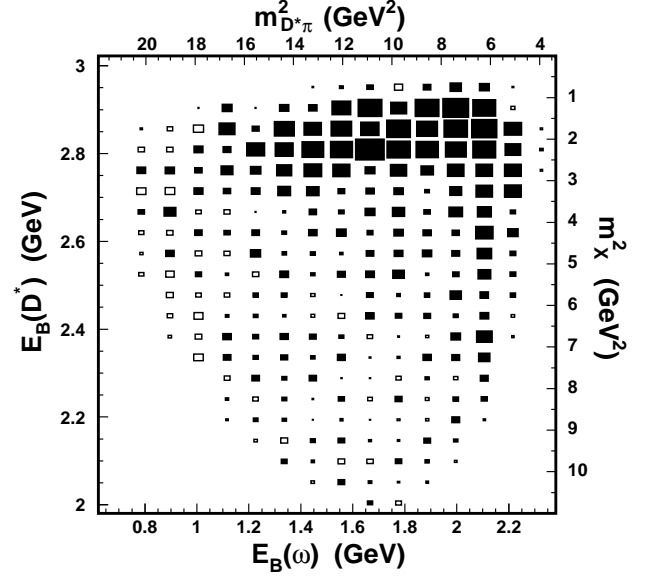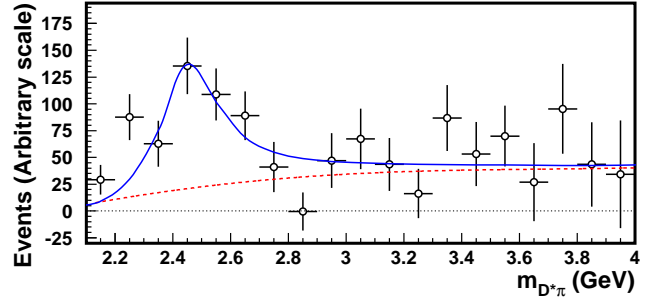
interference effects between $\overline{B}^0 \to D_1'\omega$ and $\overline{B}^0 \to D^*\omega\pi$.

The branching fraction in Eq. 4 is comparable to the branching fractions for $\overline{B}^0 \to D^{(*)0}\omega$ [8]. Also, we see no evidence for decays into the two narrow D^{**} resonances at 2420 and 2460 MeV. This is in contrast to the color-favored $B^- \to D^{**0}\pi^-$ decays, where the three D^{**} modes contribute with comparable strengths, and where the $B^- \to D_1'\pi^-$ branching fraction is one order of magnitude smaller than that of $B^- \to D^{(*)0}\pi^-$.

The presence of $\overline{B}^0 \to D_1'\omega$ would affect the comparison of the data with the theoretical predictions of Fig. 6. As can be seen in Fig. 7, $\overline{B}^0 \to D_1'\omega$ would mostly con-

tribute at high value of m_X^2, while the factorization test can be carried out only where the τ data is available; i.e., for $m_X^2 < 3$ GeV^2. Based on the estimated branching fraction of $\overline{B}^0 \to D_1'\omega$, and neglecting interference effects, the contribution of $\overline{B}^0 \to D_1'\omega$ to the $m_X^2 < 3$ GeV^2 distribution would be less than 5%.

If the decay $\overline{B}^0 \to D^{*+}\omega\pi^-$ proceeds dominantly through $\overline{B}^0 \to D^{*+}\rho(1450)$, $\rho(1450) \to \omega\pi^-$, a measurement of the polarization of the D^* can provide a further test of factorization and HQET [15]. The angular distribution in the $D^{*+} \to D^0\pi^+$ decay can be written as a function of three complex amplitudes H_0 (longitudinal), and H_+ and H_-(transverse), as

$$\frac{d\Gamma}{d\cos\theta_D} \propto 4|H_0|^2 \cos^2\theta_D + (|H_+|^2 + |H_-|^2)\sin^2\theta_D, \quad (5)$$

where θ_D is the decay angle of the D^* defined above.

The longitudinal polarization fraction Γ_L/Γ, given by

$$\frac{\Gamma_L}{\Gamma} = \frac{|H_0|^2}{|H_0|^2 + |H_+|^2 + |H_-|^2}, \quad (6)$$

can then be extracted using Eq. 5 from a fit to the angular distribution in the decay of the D^*.

We divide our dataset in ranges of m_X^2, and perform binned chi-squared fits to the efficiency-corrected, background-subtracted, D^*-decay angular distributions. In these measurements, nearly all of the systematic uncertainties discussed above cancel. As a result, the m_X^2-dependent uncertainty due to the finite Monte Carlo sample is the dominant systematic uncertainty, and typically results in an uncertainty on Γ_L/Γ at the few percent level. We also include a systematic uncertainty due to the parameter β in Eq. 2. This uncertainty is about one order of magnitude smaller.

The measured longitudinal polarization fractions as a function of m_X are presented in Table I. Near the mean of the $\rho(1450)$ resonance ($1.1 < m_X < 1.9$ GeV), we find $\Gamma_L/\Gamma = 0.654 \pm 0.042(\text{stat.}) \pm 0.016(\text{syst.})$. This result is in agreement with the previous result in the same mass range from the CLEO collaboration, $\Gamma_L/\Gamma = 0.63 \pm 0.09$. It is also in agreement with predictions based on HQET, factorization, and the measurement of semileptonic B-decay form factors, $\Gamma_L/\Gamma = 0.684 \pm 0.009$ [19], assuming that the decay proceeds via $\overline{B}^0 \to D^{*+}\rho(1450)$, $\rho(1450) \to \omega\pi^-$. These results are shown in Fig. 9.

IX. CONCLUSIONS

We have studied the decay $\overline{B}^0 \to D^{*+}\omega\pi^-$ with a larger data sample than previously available. We measure the branching fraction to be $\mathcal{B}(\overline{B}^0 \to D^{*+}\omega\pi^-) = (2.88 \pm 0.21(\text{stat.}) \pm 0.32(\text{syst.})) \times 10^{-3}$.

The invariant mass spectrum of the $\omega\pi$ system is found to be in agreement with theoretical expectations based on factorization and τ decay data. The Dalitz plot for this

TABLE I: Results of the D^* polarization measurement in bins of m_X. The first uncertainty is statistical and the second is systematic.

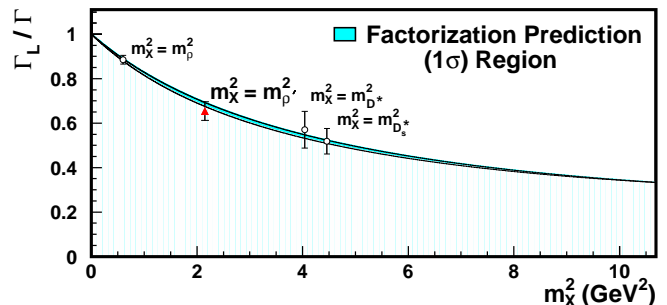| m_X range (GeV)	Γ_L/Γ
below 1.1	$0.458 \pm 0.189 \pm 0.059$
1.1 - 1.35	$0.779 \pm 0.062 \pm 0.020$
1.35 - 1.55	$0.733 \pm 0.071 \pm 0.024$
1.55 - 1.9	$0.435 \pm 0.102 \pm 0.040$
1.9 - 2.83	$0.656 \pm 0.182 \pm 0.077$

FIG. 9: The fraction of longitudinal polarization as a function of m_X^2, where X is a vector meson. Shown (as a triangle) is the $\overline{B}^0 \to D^{*+}\omega\pi^-$ polarization measurement for events with $1.1 < m_X < 1.9$ GeV ($m_X^2 = m_{\rho'}^2$, where $\rho' \equiv \rho(1450)$), as well as earlier measurements (indicated by open circles) of $\overline{B}^0 \to D^{*+}\rho^-$ [16], $\overline{B}^0 \to D^{*+}D^{*-}$ [17], and $\overline{B}^0 \to D^{*+}D_s^{*-}$ [18]. The shaded region represents the prediction ($\pm$ one standard deviation) based on factorization and HQET, extrapolated from the semileptonic $\overline{B}^0 \to D^{*+}\ell^-\bar{\nu}$ form factor results [19].

mode is very non-uniform, with most of the rate at low $\omega\pi$ mass. We also find an enhancement for $D^*\pi$ masses broadly distributed around 2.5 GeV. This enhancement could be due to color-suppressed decays into the broad D_1' resonance, $\overline{B}^0 \to D_1'\omega$, followed by $D_1' \to D^{*+}\pi^-$, with a branching fraction comparable to $\overline{B}^0 \to D^{(*)0}\omega$.

We also measure the fraction of D^* longitudinal polarization in this decay. In the region of $\omega\pi$ mass between 1.1 and 1.9 GeV, where one expects contributions from $\overline{B}^0 \to D^{*+}\rho(1450)$, $\rho(1450) \to \omega\pi^-$, we find $\Gamma_L/\Gamma = 0.654 \pm 0.042(\text{stat.}) \pm 0.016(\text{syst.})$, in agreement with predictions based on HQET, factorization, and the measurement of semileptonic B-decay form factors.

[1] J. D. Bjorken, Nucl. Phys. B Proc. Suppl. **11**, 325 (1989); M. J. Dugan and B. Grinstein, Phys Lett. **B255**, 583 (1991); H. D. Politzer and M. B. Wise, Phys Lett. **B257**, 399 (1991).

[2] Z. Ligeti, M. B. Luke, and M. Wise, Phys. Lett. **B507**, 142 (2001); C. Reader and N. Isgur, Phys. Rev. **D 47**, 1007 (1993).

[3] N. Isgur, D. Scora, B. Grinstein, and M. B. Wise, Phys. Rev. **D39**, 799 (1989); D. Scora and N. Isgur, Phys. Rev. **D52**, 2783 (1995).

[4] CLEO Collaboration, J. P. Alexander et al., Phys. Rev. **D64**, 092001 (2001).

[5] J. Korner and G. Goldstein, Phys. Lett. **B89**, 105 (1979); M. Neubert and B. Stech, in *Heavy Flavors, 2nd Edition*, edited by A. J. Buras and M. Lindner, World Scientific, Singapore, 1997.

[6] *BABAR* Collaboration, B. Aubert et al., Nucl. Inst. Methods **A479**, 1 (2002).

[7] S. Agostinelli et al., Nucl. Inst. Methods **A506**, 250(2003).

[8] Particle Data Group, S. Eidelman et al., Phys. Lett. **B592**, 1 (2004).

[9] CLEO Collaboration, S. Kopp et al., Phys. Rev. D **63**, 092001 (2001).

[10] D. H. Perkins, *Introduction to High Energy Physics*, 2nd Ed. (Addison-Wesley, Reading, 1982), p.136, 1982; B. C. Maglic et al., Phys. Rev. Lett. **7**, 178 (1961).

[11] R. A. Fisher, Ann. Eugenics **7**, 179 (1936); M. G. Kendall and A. Stuart, *The Advanced Theory of Statistics*, 2nd Ed. (Hafner Publishing, New York, 1968), Vol. III.

[12] The function is $f(m_{ES}) \propto m_{ES}\sqrt{1-x^2}\exp[-\zeta(1-x^2)]$, where $x = 2m_{ES}/\sqrt{s}$ and ζ is a fit parameter; ARGUS Collaboration, H. Albrecht et al., Z. Phys. **C48**, 543 (1990).

[13] CLEO collaboration, K. W. Edwards et al., Phys. Rev. **D61**, 072003 (2000).

[14] Belle Collaboration, K. Abe et al., Phys. Rev. **D69**, 112002 (2004).

[15] J. Körner and G. Goldstein, Phys Lett. **B89**, 105 (1979); G. Kramer and W.F. Palmer, Phys. Rev. **D45**, 193 (1992).

[16] CLEO Collaboration, S. E. Csorna et al., Phys. Rev. **D67**, 112002 (2003).

[17] Belle Collaboration, H. Miyake et al., Phys. Lett. **B618**, 34 (2005).

[18] *BABAR* Collaboration, B. Aubert et al., Phys. Rev. **D67**, 092003 (2003).

[19] *BABAR* Collaboration, B. Aubert et al., submitted to Phys. Rev. **D**, hep-ex/0602023.